

Pathways for Energy Transfer in the Core Light-Harvesting Complexes CP43 and CP47 of Photosystem II

Frank L. de Weerd, Ivo H. M. van Stokkum, Herbert van Amerongen, Jan P. Dekker, and Rienk van Grondelle
Department of Biophysics and Physics of Complex Systems, Division of Physics and Astronomy, Faculty of Sciences, Vrije Universiteit, De Boelelaan 1081, 1081 HV Amsterdam, The Netherlands

ABSTRACT The pigment-protein complexes CP43 and CP47 transfer excitation energy from the peripheral antenna of photosystem II toward the photochemical reaction center. We measured the excitation dynamics of the chlorophylls in isolated CP43 and CP47 complexes at 77 K by time-resolved absorbance-difference and fluorescence spectroscopy. The spectral relaxation appeared to occur with rates of 0.2–0.4 ps and 2–3 ps in both complexes, whereas an additional relaxation of 17 ps was observed only in CP47. Using the 3.8-Å crystal structure of the photosystem II core complex from *Synechococcus elongatus* (A. Zouni, H.-T. Witt, J. Kern, P. Fromme, N. Krauss, W. Saenger, and P. Orth, 2001, *Nature*, 409:739–743), excitation energy transfer kinetics were calculated and a Monte Carlo simulation of the absorption spectra was performed. In both complexes, the rate of 0.2–0.4 ps can be ascribed to excitation energy transfer within a layer of chlorophylls near the stromal side of the membrane, and the slower 2–3-ps process to excitation energy transfer to the calculated lowest excitonic state. We conclude that excitation energy transfer within CP43 and CP47 is fast and does not contribute significantly to the well-known slow trapping of excitation energy in photosystem II.

INTRODUCTION

Photosystem II (PSII) is a large pigment-protein complex embedded in the thylakoid membranes of green plants, algae, and cyanobacteria. The complex consists of two structurally and functionally different parts. The first is the so-called PSII core complex, which contains the photochemical reaction center (RC) bound to the D1 and D2 proteins and two sequence-related light-harvesting complexes CP43 and CP47 as its main constituents. The CP43 and CP47 complexes each bind ~14 chlorophyll *a* (Chl *a*) and 2–3 β -carotene molecules. Their main function is to transfer excitation energy into the RC (van Grondelle et al., 1994), where a charge separation is initiated. The released electrons are transferred to plastoquinone, and via the cytochrome *b₆f* complex to plastocyanin (or cytochrome *c₆* in certain cyanobacteria). The redox potential of the oxidized primary electron donor (P680⁺) is sufficiently high to oxidize water to molecular oxygen. The protons liberated during this process contribute to the transmembrane pH gradient, which provides the driving force for ATP synthesis.

The second part of PSII is formed by the peripheral antenna, which in green plants consists of a number of pigment-protein complexes of the Cab gene family, which all bind several Chl *a*, Chl *b*, and xanthophyll molecules. Some of these peripheral antenna molecules are closely associated with the PSII core complex in the PSII-LHCII supercomplexes (Boekema et al., 1999ab), the structure of which suggest that the peripheral proteins CP26 and S-

LHCII transfer their excitation energy into CP43, whereas CP29 and CP24 transfer their energy into CP47.

Trapping kinetics have been measured on PSII core complexes from various organisms (see, e.g., Schatz et al., 1988; van Grondelle et al., 1994). Most results point to trapping in open centers (in which the primary quinone acceptor Q_A is in the oxidized state) in 50–100 ps. These trapping kinetics are much slower than observed in photosystem I (PSI), the other photosystem of oxygenic photosynthesis (Gobets et al., 2001).

The crystal structure of the PSII core complex of the cyanobacterium *Synechococcus elongatus* was published at a resolution of 3.8 Å (Zouni et al., 2001). Six chlorins (four Chls and two pheophytin *a* molecules) constitute the RC, whereas 28 Chls can be regarded as core antenna chlorophylls, 14 of which are bound to CP47, 12 to CP43, and 2 to the D1/D2 complex. Further analysis of the same x-ray data showed the presence of three additional antenna Chls, of which two are bound to the CP47 and one to the CP43 complex (Vasil'ev et al., 2001). In this study, the energy transfer from CP43/CP47 to the RC was modeled, and it was suggested that trapping of excitations critically depends on a few bridging molecules, thus giving rise to the slow trapping kinetics in PSII (Vasil'ev et al., 2001).

The discussion on the origin of these slow trapping kinetics would be further clarified if the kinetics and routes of energy transfer within the PSII core antenna proteins are known. Information on the excitation dynamics in CP43 and CP47 has, as yet, been obtained only from different types of hole burning. From spectral hole-burning experiments on CP47 a 684-nm state was identified that relaxes to an exciton state at 687 nm in ~10 ps (Chang et al., 1994). The authors proposed that this 687-nm state is part of a Chl *a* dimer, which relaxes to its low-exciton state at 690 nm in 70 fs, which on its turn was proposed to dephase in ~50 ps. In

Submitted July 26, 2001, and accepted for publication November 16, 2001.

Address reprint requests to Dr. Frank L. de Weerd, Vrije Universiteit, Department of Biophysics, Division of Physics and Astronomy, De Boelelaan 1081, 1081 HV Amsterdam, The Netherlands. Tel.: 31-20-4447934; Fax: 31-20-4447999; E-mail: weerd@nat.vu.nl.

© 2002 by the Biophysical Society

0006-3495/02/03/1586/12 \$2.00

another hole-burning study (Den Hartog et al., 1998), the full power and temperature dependence of the hole widths was measured, and a linewidth corresponding to a much longer lifetime of 4 ± 1 ns was determined for the 690-nm state. In a study on CP43 (Jankowiak et al., 2000), two quasi-degenerate traps located on single Chl *a* molecules at 682.9 and 683.3 nm were reported with a width of 45 and 120 cm^{-1} , respectively, in line with earlier fluorescence line-narrowing studies (Groot et al., 1999).

In this study we present a full and systematic investigation of excitation transfer dynamics (at 77 K) in isolated CP43 and CP47 complexes with a time resolution of ~ 140 fs. For both complexes, main excitation energy transfer (EET) kinetics of 0.2–0.4 and 2–3 ps were observed. We simulated these dynamics on the basis of calculated absorption spectra, using data from the crystal structure of PSII from *Synechococcus elongatus* (Zouni et al., 2001). The results suggest routes for the main pathways of energy transfer within the CP43 and CP47 complexes and together with the available structures also provide hints for the energy transfer routes from CP43 and CP47 to the RC.

MATERIALS AND METHODS

Sample preparation

CP43 and CP47 were purified from spinach as described elsewhere (Groot et al., 1995, 1999). CP43 was dissolved in a buffer containing 0.09% (w/v) β -DM, 20 mM NaCl, 70% (v/v) glycerol, and 20 mM Hepes (pH 7.5). In the case of CP47, the Hepes in the above-mentioned buffer was replaced by BisTris (pH 6.5).

Transient absorption

Data were recorded with a femtosecond spectrophotometer, described in detail elsewhere (Gradinaru et al., 2000). The output of a Ti:sapphire oscillator was amplified by means of chirped pulse amplification (α -1000 US, B.M. Industries, Orsay, France), generating 1-kHz, 800-nm, 60-fs pulses. This light was used for generating a white light continuum in a 2-mm sapphire plate used as the probe and for driving a home-built, noncollinear optical parametric amplifier (OPA) (Wilhelm et al., 1997), tunable in the visible. After prism compression the bandwidth of excitation was limited to ~ 8 nm full width at half-maximum (fwhm) by interference filters. Parallel, magic angle, and perpendicular polarized transient absorption spectra were measured by rotating the polarization of the pump with a Berek polarization compensator (New Focus, 5540). To avoid annihilation, the excitation energy was kept low (~ 1.5 nJ/pulse). In this intensity region the transient bleach at long delay times scaled linearly with the excitation power. Time-gated spectra were recorded with a home-built camera consisting of a double diode array, read out at the laser frequency (1 kHz). Typically 2000 absorbance difference spectra were averaged per delay.

Analysis of transient absorption data

The magic-angle spectra were fitted with a global analysis fitting program (van Stokkum et al., 1994). An irreversible sequential model with increasing lifetimes was assumed where each species-associated difference spectrum (SADS) evolves into the next one. Note that these SADS in general

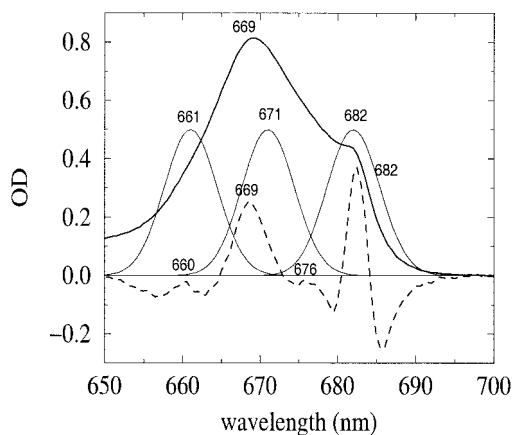


FIGURE 1 Absorption spectrum (—) and second-derivative spectrum (multiplied by -10 , ---) of CP43 at 77 K. Also shown are the spectral profiles (fwhm 8 nm, —) of the pump pulses used in the transient absorption experiments.

reflect mixtures of states and are only used as a means to describe the spectral evolution present in our data. Parallel to this evolution, a spectral feature around time 0 was fitted to account for the coherent coupling between pump and probe pulses (Monshouwer et al., 1998). The time profile of this feature in our fitting procedure was fixed to the instrument response function. Dispersion within the probe continuum was accounted for by a third-order polynomial, derived from the induced absorption change in styryl9M. The obtained parameters agreed very well with those found for several experiments performed under similar conditions and were fixed in our fitting procedure. The instrument response function was described by a Gaussian with the fwhm as a fitting parameter (0.12–0.15 ps).

Transient fluorescence

The samples were excited using nonselective 100–200-fs pulses at 400 nm at a repetition rate of 20 kHz (50 nJ/pulse). The laser beam was not focused in the sample, limiting the instrument response (~ 9 ps fwhm). Time-resolved fluorescence spectra were detected under magic angle with respect to the excitation light with a Hamamatsu C5680 synchroscan streak camera (Gobets et al., 2001). The bandwidth of detection was 3–4 nm. Like for the transient absorption, the fluorescence data were analyzed globally with a sequential model. The backsweep of the streak camera was used to estimate the nanosecond fluorescence decay times.

RESULTS AND DISCUSSION

Sub-picosecond transient absorption in CP43

The 77 K absorption spectrum in the Q_y region of the purified CP43 antenna complex is shown in Fig. 1. Our spectrum is in good agreement with low-temperature literature spectra, which display bands at 660, 669, and ~ 679 nm and a sharp and small band at ~ 682.5 nm (Groot et al., 1999; Jankowiak et al., 2000). Absorption difference spectra were measured in the purified CP43 antenna complex at 77 K upon excitation around 661, 671, and 682 nm for delay times of 0–500 ps between pump and probe. The bandwidth of excitation was 8 nm (fwhm) and is compared with the

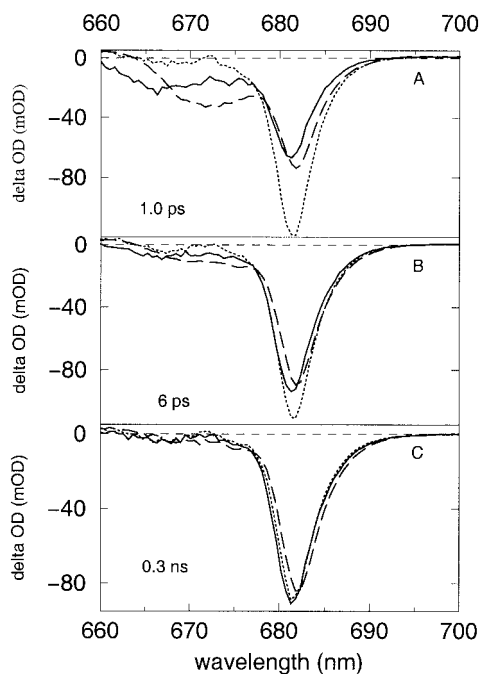


FIGURE 2 Time-gated spectra of CP43 after excitation (77 K, fwhm 8 nm) at 661 nm (—), 671 nm (---) and 682 nm (···). Pump was set to magic angle relative to the probe. (A) Pump-probe delay 1.0 ps; (B) Delay 6 ps; (C) Delay 0.3 ns. The spectra for the three excitation wavelengths have been normalized with respect to each other based on the area after 6 ps (second panel).

spectral width of the Q_y band in Fig. 1. Fig. 2 shows magic-angle absorption difference spectra, recorded at various delay times after excitation around 661 nm (solid line), 671 nm (dashed line), and 682 nm (dotted line). The spectra for the three excitation wavelengths have been normalized with respect to each other based on the area after 6 ps (Fig. 2 B). Fig. 2 A (1.0 ps) exhibits for all the excitation wavelengths a relatively sharp bleaching/stimulated emission (SE) component around 682 nm. In the case of the 661- and 671-nm excitation, this component is populated due to a subpicosecond relaxation from the initially populated bands (see below). Nevertheless, following 661- and 671-nm excitation, considerable bleaching/SE is still present around 670 nm after 1 ps. Subsequently, most of this remaining bleaching/SE is lost within a few picoseconds and also transferred to the 682-nm component on this timescale (Fig. 2 B, 6 ps). For all excitation wavelengths, the difference spectra remain narrow and symmetric on a longer timescale and peak at 682 nm in all cases (Fig. 2 C, 0.3 ns). The observed relaxation will now be discussed for each excitation wavelength individually.

Excitation at 671 nm

More details of the magic-angle data upon excitation in the main Q_y absorption band around 671 nm are shown in Fig.

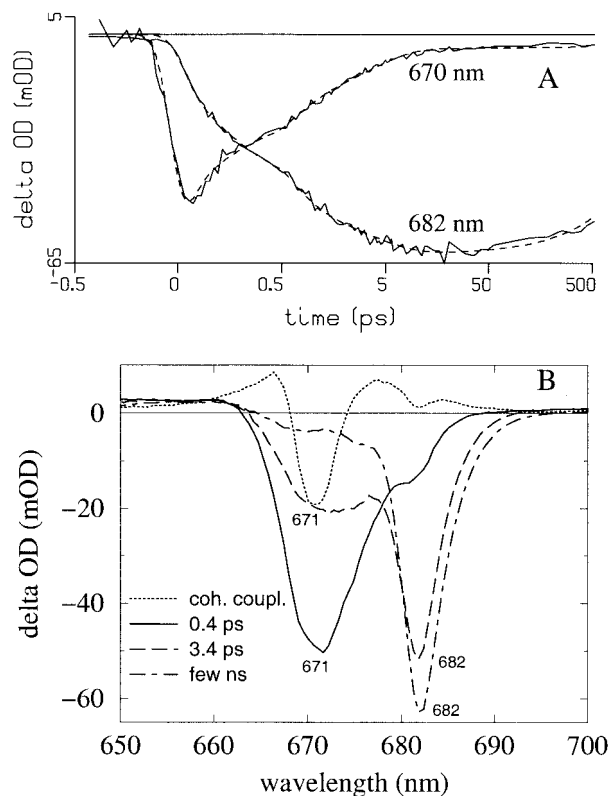


FIGURE 3 Pump-probe data (77 K) and global analysis fit for CP43 after 671 nm excitation (fwhm 8 nm). Pump was set to magic angle relative to the probe. (A) Traces recorded at 670 nm and 682 nm are shown with data (—) and global analysis fit (---), corrected for the dispersion. Note that the time axis is linear between -0.5 and 0.5 ps and logarithmic at later delay times. The instrument response time is 0.15 ps. (B) SADS and connecting lifetimes resulting from the global fit. The first SADS (—) is the fitted spectrum at time 0, which is replaced by the second SADS (---) on a 0.4-ps timescale, and so on. Parallel to this evolution a coherent coupling (···) between pump and probe pulses was fitted (see text).

3. In addition to the experimentally observed difference spectra in Fig. 2, experimentally observed traces at two representative wavelengths (Fig. 3 A, solid lines) are displayed together with the result of a global analysis fit to the data (Fig. 3 A, dashed lines). This global analysis fit represents a good description of the measured traces. Three SADS were required for this global analysis fit (Fig. 3 B).

The dotted spectrum in Fig. 3 B represents the fitted coherent coupling between pump and probe pulses and exhibits a negative absorption difference at the excitation wavelength and positive values on either side. The first SADS (solid line) represents the absorption difference spectrum at time 0. It shows a bleaching/SE at 671 nm and weak excited-state absorption (ESA) below 663 nm. The absorption around 660 nm does not show a bleach, suggesting a nonvibronic origin of this band. The second SADS (dashed line) arises from the first with a 0.4-ps time constant. On this timescale, about half of the bleaching/SE around 671

nm is lost and transferred to a relatively sharp bleaching/SE component at 682 nm. No significant spectral changes occurred below 663 nm on this timescale. The second SADS is then replaced by the third SADS (dot-dashed line) with a 3.4-ps time constant. Most of the remaining bleaching/SE around 671 nm is lost and further builds up around 682 nm. The transition from the second to the third SADS has a slight nonconservative character, meaning that the gained bleaching/SE does not completely match the lost bleaching/SE. The third SADS is centered around 682 nm and has additional minima around 670 and 675 nm. No further spectral evolution was observed. The lifetime of the third SADS (several nanoseconds) could not be precisely determined, because difference spectra were not measured for delay times longer than 0.5 ns.

Excitation at 661 nm

Upon excitation into the blue wing of the Q_y absorption band (around 661 nm), the magic-angle difference spectrum exhibits a broad minimum around 665 nm at time 0 (not shown). Most of this bleaching/SE is lost on a subpicosecond timescale and transferred to the 682-nm component. After ~ 1 ps (see first panel in Fig. 2) the difference spectrum still exhibits a (local) minimum around 665 nm and differs significantly from the spectrum obtained upon exciting around 671 nm. Nevertheless, the bi-exponential ingrowth of the red component after 661- and 671-nm excitation is very similar. The final difference spectrum peaks at 681.5 nm and displays additional minima around 667 and 675 nm. The described relaxation upon excitation around 661 nm could be fitted globally with three SADS (not shown) and connecting lifetimes of 0.4 and 2.8 ps.

Excitation at 682 nm

Upon exciting into the red wing of the Q_y absorption band (around 682 nm), only small spectral changes could be observed in the magic-angle data (see Fig. 2). This data could reasonably well be fitted with two SADS (not shown) with a connecting lifetime of 2.6 ps. This rate reflects a nonconservative relaxation from pigments absorbing around 679 nm to more red-absorbing pigments. The final difference spectrum is essentially identical to the one after excitation around 661 nm (see Fig. 2 C), peaking at 681.5 nm (fwhm 5 nm) and displaying additional minima around 667 nm and 675 nm. At intermediate wavelengths (665–675 nm) the anisotropy upon excitation around 682 nm was negative at all times. Magic-angle (solid line), parallel (dotted line), and perpendicular (dashed line) polarized spectra at the latest time point (0.5 ns) following 682-nm excitation are shown in Fig. 4. The anisotropy in the region 665–675 nm should be interpreted with care, because the transient absorption signals are small and canceling absorption changes can hinder the interpretation (our data could orig-

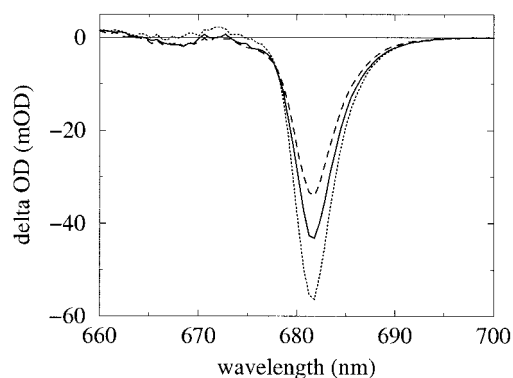


FIGURE 4 Absorption difference spectra at a time delay of 0.5 ns in CP43 after 682-nm excitation (77 K, fwhm 8 nm), with magic angle (—), parallel (· · ·), and perpendicular (---) polarization of the pump relative to the probe.

inate from an ESA with positive anisotropy plus an isotropic bleaching/SE). The most natural explanation, however, would be that dipoles with an orientation perpendicular to the initially excited dipoles are bleached, indicating an excitonic coupling between the 667-, 675-, and 682-nm states.

Sub-picosecond transient absorption in CP47

The 77 K absorption spectrum in the Q_y region of the CP47 complex is shown in Fig. 5. Our spectrum is in good agreement with low-temperature literature spectra, which display bands at ~ 661 , ~ 670 , ~ 677 , ~ 683 , and ~ 690 nm (van Dorssen et al., 1987; Chang et al., 1994; Groot et al., 1995). The amplitude of the 690-nm component is small, but its presence is apparent from the long-wavelength tail of the spectrum. Absorption difference spectra were measured in the purified CP47 antenna complex at 77 K after excita-

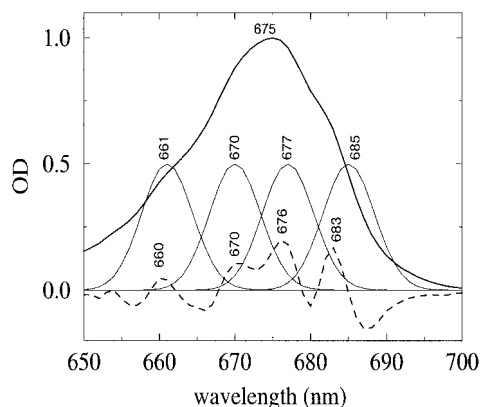


FIGURE 5 Absorption spectrum (—) and second-derivative spectrum (multiplied by -10 , ---) of CP47 at 77 K. Also shown are the spectral profiles (fwhm 8 nm, —) of the pump pulses used in the transient absorption experiments.

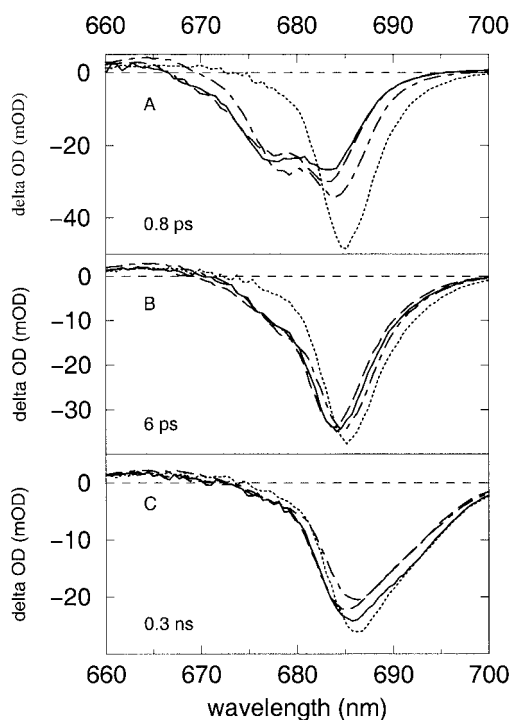


FIGURE 6 Time-gated spectra of CP47 after excitation (77 K, fwhm 8 nm) at 661 nm (—), 670 nm (---), 677 nm (— · —), and 685 nm (· · ·). Pump was set to magic angle relative to the probe. (A) Pump-probe delay 0.8 ps; (B) Delay 6 ps; (C) Delay 0.3 ns. The spectra for the four excitation wavelengths have been normalized with respect to each other based on the area after 6 ps (second panel).

tion around 661, 670, 677, and 685 nm for delay times of 0–500 ps between pump and probe. The bandwidth of excitation was 8 nm (fwhm), as for the experiments on the CP43 complex (see above), and is visualized in Fig. 5. Fig. 6 shows magic-angle absorption difference spectra, recorded at various delay times after excitation around 661 nm (solid line), 670 nm (long-dashed line), 677 nm (dot-dashed line), and 685 nm (dotted line). The spectra for the four excitation wavelengths have been normalized with respect to each other based on the area after 6 ps (Fig. 6 B). We interpreted the excited-state dynamics in terms of the bands obtained from the deconvolution of the steady-state absorption spectrum. Except for the red-most excitation, the population of excited states is distributed over the 677- and 683-nm components with a subpicosecond time constant (Fig. 6 A, difference spectra after 0.8 ps). In contrast to CP43, almost all bleaching/SE around 670 nm has been lost on this timescale. Subsequently, bleaching/SE around 677 nm is lost and replaced by the 683-nm component within a few picoseconds. The state reached after a few picoseconds is almost identical for all excitation wavelengths (Fig. 6 B, 6 ps), except for the red-most excitation wavelength. In contrast to CP43, a further spectral evolution occurs on a longer timescale; the difference spectra become asymmetric (Fig. 6 C, 0.3 ns).

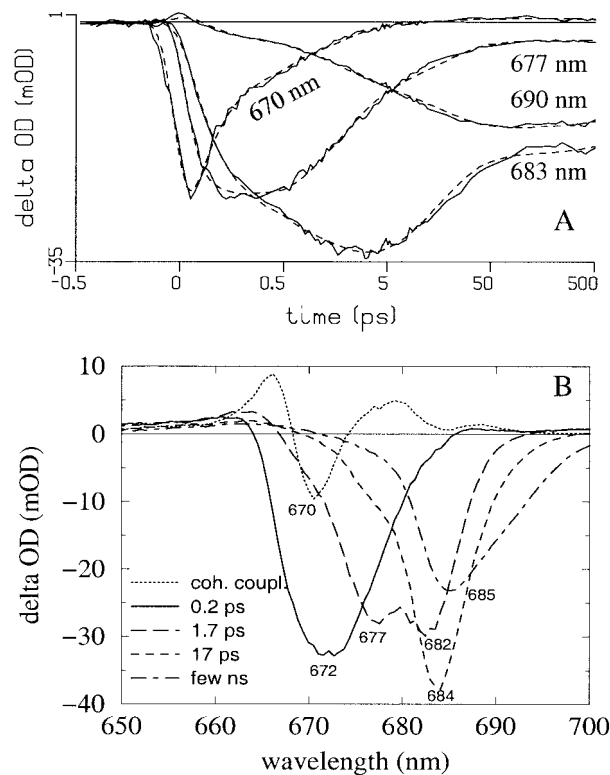


FIGURE 7 Pump-probe data (77 K) and global analysis fit for CP47 after 670-nm excitation (fwhm 8 nm). Pump and probe were set to magic angle. (A) Traces recorded at 670, 677, 683, and 690 nm are shown with data (—) and global analysis fit (---), corrected for the dispersion. Note that the time axis is linear between -0.5 and 0.5 ps and logarithmic at later delay times. The instrument response time is 0.14 ps. (B) SADS and connecting lifetimes resulting from the global fit. The first SADS (—) is the fitted spectrum at time 0, which is replaced by the second SADS (---) on a 0.2-ps timescale, and so on. Parallel to this evolution a coherent coupling (· · ·) between pump and probe pulses was fitted (see text).

Excitation at 670 nm

More details of the magic-angle data upon excitation around 670 nm are shown in Fig. 7. In addition to the experimentally observed difference spectra in Fig. 6, we show experimentally observed traces at a variety of representative wavelengths (solid lines) in Fig. 7 A, together with the result of a global analysis fit to the data (dashed lines). The global analysis fit yields an adequate description of the data. Four SADS were required for this fit (Fig. 7 B), of which the first three are strongly reminiscent of the three SADS needed to describe the spectral evolution in CP43 after 671-nm excitation (Fig. 3 A). The first SADS (Fig. 7 B, solid line) represents the absorption difference spectrum at time 0 and exhibits a broad bleaching/SE around 672 nm and ESA below 663 nm. The spectrum around 660 nm does not show a bleach, suggesting a nonvibronic origin of this band. The fitted coherent coupling between pump and probe pulses (dotted line) has a similar spectrum and origin as described

before for CP43. Here, it imposes some difficulty in the precise fitting of the first SADS because of the somewhat faster spectral evolution that takes place in CP47. Following the formation of the initial population of excited states, the first SADS (solid line) is replaced by the second SADS (long-dashed line) with a time constant of 0.2 ps. The bleaching/SE around the 672-nm state is almost completely lost with this time constant and replaced by two bands around 677 and 683 nm. The spectral changes associated with this process have a conservative character. The third SADS (short-dashed line) arises from the second SADS with a time constant of 1.7 ps and describes the consecutive transfer from the 677-nm component to the 683-nm component (which seems slightly red-shifted compared with the 683-nm component that arises after 0.2 ps). The fourth SADS (dot-dashed line) arises then with a much longer time constant (17 ps) and is associated with a partial relaxation from the Chls that were bleached at 677 nm and 683 nm to a Chl absorbing at even lower energy. The transition from the third to the fourth SADS has a strongly nonconservative character. The fourth SADS (nanoseconds lifetime) peaks at 685 nm, is asymmetric (fwhm 11 nm), and shows no distinct bleach of higher-energy states. No further spectral evolution takes place up to 0.5 ns.

Excitation at 661 nm and 677 nm

Following the formation of the initial population of excited states, a subpicosecond relaxation to bands at 677 and 683 nm occurs. As shown in Fig. 6, the magic-angle difference spectra at delay times of 0.8 ps and longer following 661- and 677-nm excitation are comparable to the case of 670-nm excitation. For both data sets, the observed dynamics could be described with the same number (four) of SADS (not shown) and similar connecting lifetimes (661-nm excitation: 0.3, 1.9, and 18 ps; 677-nm excitation: 0.2, 2.2, and 18 ps) compared with the 670-nm excitation. These observations differ from those on CP43, where the difference spectra upon excitation around 661 and 671 nm are still different after ~ 1 ps.

Excitation at 685 nm

Upon exciting into the red wing of the Q_y band (around 685 nm), the magic-angle difference spectrum at time 0 exhibits a bleaching/SE around 685 nm. It does not change much on a few-picoseconds timescale (see Fig. 6, dotted lines). On a longer timescale, a similar spectral relaxation is observed as after excitation at 661, 670, and 677 nm.

As we did for the CP43 data after red-most excitation (Fig. 4), magic-angle (solid line), parallel (dotted line), and perpendicular (dashed line) polarized spectra of CP47 at the latest time point following 685-nm excitation are displayed in Fig. 8 C, together with traces recorded at 678 (Fig. 8 A) and 685 (Fig. 8 B) nm. On the very blue side (< 670 nm), the

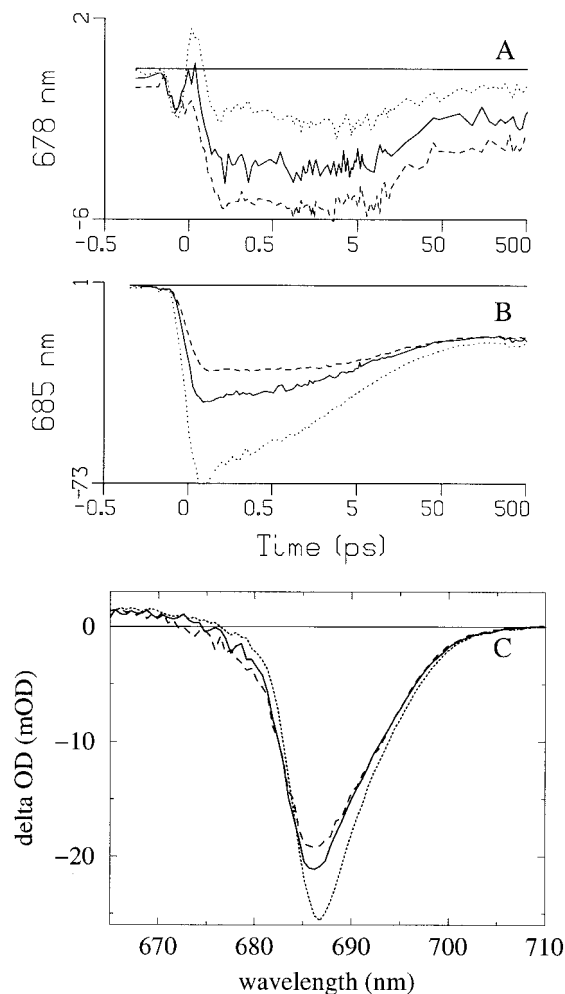


FIGURE 8 Pump-probe data of CP47 after 685-nm excitation (77 K, fwhm 8 nm), with magic angle (—), parallel (\cdots), and perpendicular (---) polarization of the pump relative to the probe. (A) Traces recorded at 678 nm; (B) Spectra recorded at 685 nm; (C) Spectra recorded at a time delay of 0.5 ns.

transient signals originate from ESA only and are small (~ 1 mOD). On the blue side of the main bleaching/SE, the data were negatively polarized at all times (see traces recorded at 678 nm in Fig. 8 A). In line with our conclusions for CP43, this suggests an excitonic coupling with the initially excited bleaching/SE component around 683 nm.

Picosecond transient fluorescence in CP47

Time-resolved fluorescence experiments at 77 K were performed to obtain more information on the slow spectral relaxation in CP47. Upon excitation into the Soret band of a Chl *a* molecule, a subpicosecond relaxation to the Q_y state occurs. These very fast rates could not be detected because of a limited instrument response time of the streak camera (~ 9 ps fwhm). In Fig. 9, we show experimentally observed traces at three representative wavelengths (inset), together

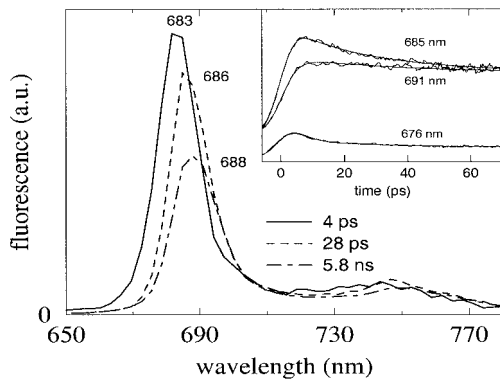


FIGURE 9 SAES and connecting lifetimes resulting from a global fit of CP47 fluorescence data after 400-nm excitation (77 K). The first SAES (—) is the fitted spectrum at time 0, which is replaced by the second SAES (---) on a 4-ps timescale, and so on. Fluorescence was detected under magic angle with respect to the excitation light. The instrument response time is ~ 9 ps. The inset shows three typical traces (data and fit), corrected for the dispersion.

with the result of a global analysis fit to the data. Three species-associated emission spectra (SAES), with connecting lifetimes of 4 and 28 ps, were required for this fit and are displayed in Fig. 9. These rates are slightly slower than those observed in the pump-probe experiments (~ 2 and ~ 17 ps). The 4-ps time constant is associated with the loss of blue fluorescence (see also the trace at 676 nm, inset) and the gain of red fluorescence and therefore suggests an EET process. The 28-ps process, however, seems to be a combination of a further red shift plus a loss of intensity, in line with the observations in the pump-probe data (see Discussion). No further slow equilibration between the two red components (683 and 690 nm) was observed in the fluorescence. The lifetime of the third SAES was fitted with a 5.8 ± 0.1 -ns time constant, slightly longer than the value of 4 ± 1 ns, obtained from spectral hole burning between 1.2 and 4.2 K (Den Hartog et al., 1998). The shape of the third SAES (peak 687–688 nm) perfectly matches the steady-state fluorescence at 77 K (fwhm 16 nm).

Modeling the absorption properties of CP43 and CP47

Structure

To understand the structural basis of the new results on the excitation transfer dynamics in CP43 and CP47, a model is needed for the spectroscopic properties of the Chls in these complexes. A structure of the PSII core complex of *Synechococcus elongatus* was published at a resolution of 3.8 Å (Zouni et al., 2001). Three additional antenna Chls and dipole orientations of all Chls are specified in a structure based on the same x-ray data (Vasil'ev et al., 2001). However, at the present resolution of 3.8 Å these dipole assignments are questionable and are not consistent with averaged orientations obtained from linear dichroism experiments on CP43 (Groot et al., 1999) and CP47 (van Dorssen et al., 1987; De Weerd, unpublished observations). Therefore, we used the positions and orientations of the heme planes of the Chls in the 3.8-Å structure of the PSII core complex of *S. elongatus* (Zouni et al., 2001) for the modeling of the spectral properties of CP43 and CP47. Fig. 10 shows these Chls, viewed along the membrane plane. The pigment organization is characterized by an empty region around the RC and by an arrangement of the Chls in two layers near the stromal and luminal sides of the membrane. Most Chl planes are oriented perpendicularly with respect to the membrane plane. The Chl organization of CP47 (14 Chls) is similar to that proposed before by Barber and coworkers on the basis of an 8-Å structure (Rhee et al., 1998; Barber et al., 2000) for CP47 of spinach, where also 14 Chls have been identified. The Chl arrangements in CP43 (12 Chls) and CP47 (14 Chls) are rather similar. In total, 11 CP43-CP47 Chl pairs exist, which correspond in terms of position and orientation of the pigment planes. The other Chls are number 34 (CP43) and numbers 39, 44, and 45 (CP47). The total number of Chls in the structure of the PSII core (32) is close to the value of 31 found spectroscopically for the same species (Dekker et al., 1988) and the value of 35 found biochemically for spinach (van Leeuwen et al., 1991). It is very well possible that a few (peripheral) Chls are missing

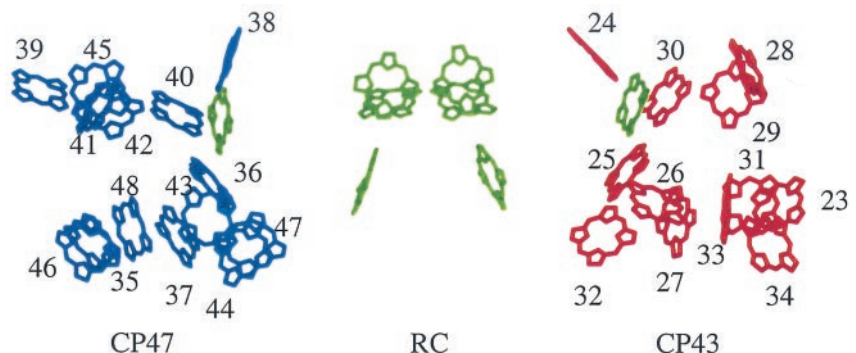


FIGURE 10 Structure of the monomeric PSII core complex looking along the plane of the membrane (taken from Zouni et al., 2001). Luminal side is at the top; stromal side is at the bottom. Green represents the RC, blue represents CP47, and red represents CP43. Note the organization of the CP43 and CP47 Chls in two layers near the stromal and luminal sides of the membrane.

TABLE 1 Close Chl pairs in CP43 and CP47

	CP43		CP47	
	Chls	Å	Chls	Å
Stroma	25–27	9.8	36–37	8.9
Stroma	27–32	10.3	37–47	9.8
Stroma	23–33	8.5	35–48	9.0
Stroma	31–34	9.9		
Lumen			39–42	9.5
Lumen			41–45	9.0

Antenna Chls from the PSII core crystal structure (Zouni et al., 2001) with a center-to-center distance of less than 10.5 Å. Each row gives a pair at corresponding positions in CP43 and CP47.

in the structure that we use for our calculations, also because three additional Chls have been proposed in another structure based on the same x-ray data (Vasil'ev et al., 2001). We therefore stress that the following calculations should be considered as a preliminary modeling attempt.

Absorption properties

The antenna proteins CP43 and CP47 exhibit distinct absorption spectra characterized by a specific set of transitions (van Dorssen et al., 1987; Chang et al., 1994; Groot et al., 1995, 1999; Den Hartog et al., 1998; Jankowiak et al., 2000). Monomeric chlorophyll in a detergent solution at 77 K exhibits a single low-energy electronic (Q_y) transition at 670 nm with a fwhm of 17 nm (Kwa et al., 1994). The fine structure and blue/red shifts of the Chl transitions in a protein may find their origin either from specific pigment-protein interactions (nearby charged residues, degree of coordination of the central Mg atom, or H-bonding to side groups) or from interactions (excitonic or charge transfer) between the pigments. That excitonic interactions may play an important role in determining the spectroscopic features in CP43 and CP47 can be inferred from the relatively intense and conservative circular dichroism spectra that both complexes exhibit in their Q_y spectral regions (Kwa et al., 1994; Groot et al., 1999). The published crystal structure of the core of PSII does not provide insight into the site energies of each of the Chls in CP43 and CP47, but within certain limits estimates for the excitonic couplings may be obtained. It follows from the PSII core structure that both in CP43 and in CP47 pairs of Chl exist with a center-to-center distance of less than 10.5 Å. These pairs represent likely candidates involved in excitonic interactions and are listed in Table 1, where each row gives a pair at corresponding positions in CP43 and CP47. Note that the stromal side of each complex contains three close pairs at equivalent positions with an additional pair in CP43, whereas CP47 contains two close Chl pairs at its luminal side, which are absent in CP43.

Monte Carlo modeling

To model the absorption spectra we have taken the following general approach. We have put the average site energy for all the pigments at 670 nm. To calculate real absorption spectra we have included inhomogeneous broadening by assuming that for each Chl the site energy is randomly taken from an inhomogeneous distribution function (IDF). From the crystal structure only the orientation of the normal to the chlorin plane is known for each of the Chls, which allows any orientation of the Q_y dipole in this plane. However, linear dichroism experiments on CP43 (Groot et al., 1999) and CP47 (van Dorssen et al., 1987; De Weerd, unpublished observations) put most of the oscillator strength at an angle to the normal of the membrane plane larger than the magic angle, except for the red transition at 690 nm in CP47. Therefore, in our first and most simple attempt we have put all the Q_y transitions in the plane of the membrane (as a result, we will not be able to reproduce the 690-nm state of CP47). The spectra are then calculated following a Monte Carlo procedure, described in detail elsewhere (Fidder et al., 1991; Monshouwer et al., 1997; van Amerongen and van Grondelle, 2001). The site energies are randomly taken from a Gaussian centered at $14,925 \text{ cm}^{-1}$ (670 nm) with a fwhm of 200 cm^{-1} . This IDF also accounts for some homogeneous broadening. The width of the IDF is slightly bigger than the value of 160 cm^{-1} used in a similar simulation of the LHCII absorption (van Amerongen and van Grondelle, 2001). The off-diagonal couplings V_{ij} between any pair of Chl molecules are then calculated using the dipole-dipole approximation given by

$$V_{ij} = \frac{5.04\kappa}{R^3} \times \frac{f_1^2 \mu^2}{\epsilon_r}, \quad (1)$$

where R is the distance between the centers of the pigments and κ is the orientation factor with possible values between -2 and 2 . The effective oscillator strength $(f_1^2 \mu^2)/\epsilon_r$ of Chl a was set to 24 D^2 (close to the value of 23 D^2 in Durrant et al., 1995). Typically, the results of $\sim 10^6$ iterations were summed and no homogeneous lineshape was included.

Using these simple assumptions, the calculated CP43 and CP47 spectra display two main absorption maxima (see Fig. 11), one located at ~ 670 nm and one red-shifted transition located at 684 nm for CP43 and at 680 nm for CP47. Because the Chls in both complexes are organized in two layers, one near the stromal side and one near the luminal side, we have repeated the same calculation for only those groups of Chls. Apart from one Chl, which is almost in the middle of the membrane (number 36 in CP47, number 25 in CP43; both counted as a stromal Chl), the center-to-center distance between any pair of Chls located in the two different layers is more than 15 Å, and consequently the two layers will display almost independent absorption characteristics.

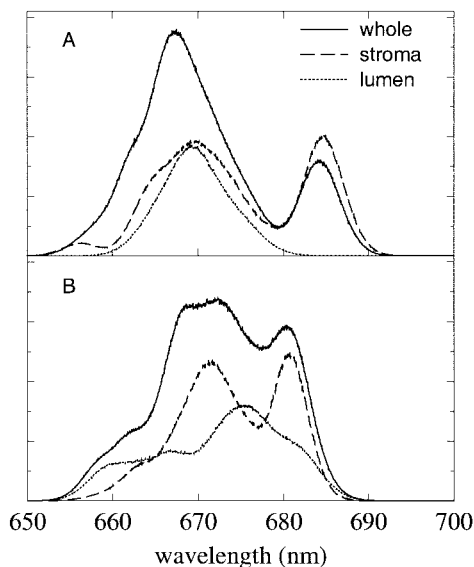


FIGURE 11 Monte Carlo simulation (—) of absorption spectra of CP43 (A) and CP47 (B). The same calculation was repeated for the stromal (---) and luminal (···) Chls only. See text for details.

CP43

For CP43, the lumen spectrum (four Chls) shows a single peak, slightly to the blue of the original monomer transition. The stromal spectrum (eight Chls) displays two peaks, again one at ~ 670 nm with a blue shoulder and a single exciton transition near 684 nm. The overall spectrum is, in a first approximation, the sum of the stromal and luminal absorption spectra. Its characteristics bear an overall resemblance to the experimental spectrum; i.e., both contain a major peak near 669 nm, a shoulder near 661 nm, and at least one red-shifted transition in the 680-nm region, in approximately the right ratio. From this modeling we conclude that the intense band near 669 nm has equal contributions from stromal and luminal sides, whereas the red band is uniquely due to stromal absorption. In experimental work two red-trap states have been identified, with reported widths of 60 and 210 cm^{-1} (Groot et al., 1999) and 45 and 120 cm^{-1} (Jankowiak et al., 2000). In the latter work, it is argued that both states are highly localized on a single Chl, and it is suggested that they are located on opposite sides of the membrane. From an examination of the eigenvectors belonging to our red-shifted CP43 state, it follows that this state is delocalized over the Chls 23, 27, and 33. We conclude that the calculated lowest exciton state reproduces the large absorption in the 680-nm region of the absorption spectrum. However, it is not certain if one of the other exciton states can account for a second trap state. We note that the coupling and therefore the delocalization is not large enough to obtain the sharp 682.5-nm transition of CP43 by exchange narrowing, given the width of the IDF that we assumed.

CP47

For CP47, the stromal absorption shows a band near 670 nm and a red-shifted state near 681 nm (due to coupling between Chls 35 and 48). This absorption is similar to that of CP43, as can be expected because of the strong match between Chl pairs in the CP43 and CP47 stromal sides (Table 1). This strongest coupling among the stromal Chls in CP47 is a bit weaker than in CP43, resulting in a smaller red shift. The luminal part of CP47 has two additional Chls (numbers 39 and 45) compared with CP43, and both are involved in strong pairwise interactions: Chl 39 with Chl 42 and Chl 45 with Chl 41. In our model this induces a red shift (compared with CP43) of the luminal absorption. For the whole CP47 complex, as in CP43, the overall spectrum can be approximated by the sum of the stromal and luminal absorption. In our simulation, the Chl 44–47 pair on the stromal side and the 41–45 pair on the luminal side contribute mostly to the third and fourth lowest exciton level and may give rise to the 677-nm band. The Chl 35–48 pair on the stromal side and the 39–42 pair on the luminal side contribute to the two lowest exciton levels and may give rise to the 683-nm band. Depending on the specific realization of the disorder, either the stromal or the luminal state is the lowest one. The result for CP47 is in overall agreement with the experimental absorption spectrum, which displays main bands at 660, 670, 677, and 683 nm. We note that a red-site energy with a different orientation is needed to explain the 690-nm state of CP47.

Concluding remarks

The Monte Carlo results for CP43 and CP47 depend on the choice of the dipole orientations. However, keeping all Q_y dipoles at an angle to the normal of the membrane plane larger than the magic angle, the main bands can shift by up to 1–2 nm and the relative amplitudes can change, but all main features remain preserved. We wish to emphasize that we explained the most prominent features in the absorption spectra of CP43 and CP47 by taking a similar site energy distribution for all the Chls. This yields states at approximately the same position and in approximately the same relative ratio as experimentally observed, suggesting that excitonic interactions (taking a realistic value for the coupling) are sufficient to explain most features.

Linking structure and excited-state dynamics in CP43 and CP47

CP43

Upon exciting the CP43 antenna near its absorption maximum around 671 nm, we observed that about half the excitations of the 670-nm component are transferred to the 682-nm component on a 0.4-ps timescale and the other half on a 3-ps timescale. Based on the conclusions from our

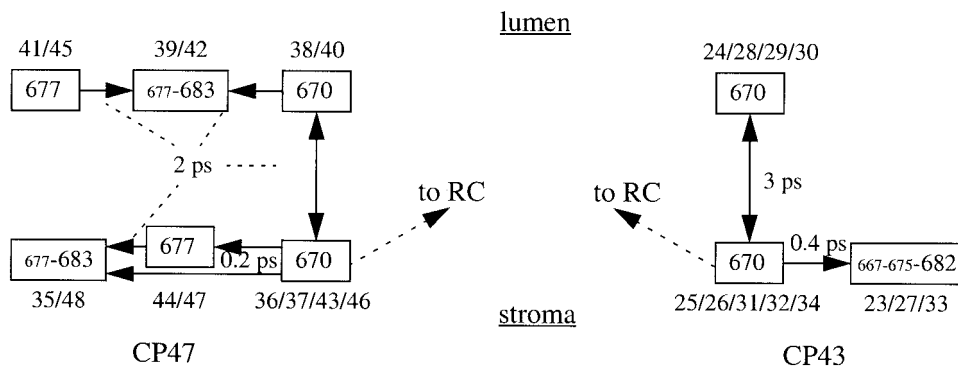


FIGURE 12 Model of excitation energy transfer (EET) pathways between groups of Chls within the PSII core. Assignment to specific groups of Chls, represented by the mean absorption wavelength, results from a simulation of the absorption spectra. The Chls contributing to each group are specified (numbered as done in Fig. 10). Given timescales and wavelengths were obtained from our transient absorption measurements. Arrows indicate downhill transfer events. Excitations in CP47 can be transferred to a red state at 690 nm (origin and localization not known). Because the simplest assumptions were taken, the assignment is not unique (see text). Also shown (*dashed arrows*) are the most likely EET routes to P680 (see text for details).

Monte Carlo simulations, we assign the 0.4-ps time to a relaxation to the lowest state within the stromal side of the membrane (located on Chls 23 and 33) and the 3-ps time to relaxation from the luminal to the stromal side. To estimate if the observed rates are consistent with the structure of CP43 we have calculated the rate of energy transfer between pigments according to the Förster equation (van Amerongen and van Grondelle, 2001). Although this may probably not be correct for energy transfer between the Chls involved in the strongly coupled pairs yielding the red states, it will provide a reasonable estimate for the more weakly coupled pigments. Then the rate of energy transfer k_{DA} is given by

$$k_{\text{DA}} = \frac{C_{\text{DA}}}{n^4} \times \frac{\kappa^2}{R_{\text{DA}}^6} \quad (2)$$

with the refractive index n taken to be equal to 1.55 (Gradinaru et al., 1998). The constant C_{DA} includes the overlap integral and was set to $32.26 \text{ ps}^{-1} \text{ nm}^6$ (Gradinaru et al., 1998). A time-dependent Stokes' shift is not included, because we do not model ultrafast (<200 fs) transfer times. Assuming all the transition dipole moments to be oriented in the plane of the membrane, the fastest interlayer rates are ~ 3 ps (between Chls 30 and 27 and also between Chls 29 and 31), in agreement with our interpretation. In general, summing the rates over all stromal Chls does not significantly speed up the interlayer rate from a specific luminal Chl. In Fig. 12, we have schematically summarized the way we associated the rates observed in our transient absorption measurements to relaxation between groups of Chls. The right side of Fig. 12 represents CP43. This scheme should, however, be interpreted with care, because a quasi-degenerate second trap state, which would not show up in our transient absorption data, could complicate this picture. We note that the number of bands in the final spectrum (three) is consistent with our modeling in which the red-shifted state is obtained by three interacting pigments.

CP47

The spectral relaxation observed upon excitation at 661, 670, and 677 nm appeared to be very similar. The second SADS (representing the difference spectrum that is formed after the 0.2-ps relaxation) displayed a 60:40 distribution over the 677- and 683-nm components (see Fig. 7 B for the 670-nm excitation). We conclude that most of the blue components (661 and 670 nm) equilibrate with the 683- and part of the 677-nm component on a 0.2-ps timescale. From preliminary calculations on transfer rates, again using the Förster equation, it follows that most of the Chls within the stromal layer are interconnected with subpicosecond energy transfer times. It also follows that within the luminal side not much subpicosecond energy transfer can occur. Therefore, we propose that the observed 0.2-ps rate reflects relaxation within the stromal side.

The 677-nm component was shown to transfer its excitation energy to the 683-nm component on a 2-ps timescale. From the calculation of transfer times, we obtained a 1.6-ps transfer time between the two luminal Chls 41 and 42 and a 1.4-ps time between Chls 40 and 42. The fastest calculated interlayer rate was 3 ps (between Chls 37 and 40). These possible pathways for the observed 2-ps EET event are shown on the left side of Fig. 12, representing CP47. This scheme should, however, be interpreted with great care. Due to the uncertainties in our simulation (i.e., real dipole orientations and possible specific site energies not known), we cannot unambiguously assign the experimentally observed rates to specific (groups of) Chls. However, we can conclude that following the ultrafast relaxation on the stromal side, the observed 2-ps phase represents relaxation to the calculated lowest state, either the Chl 39–42 pair on the luminal or the Chl 35–48 pair on the stromal side.

A slower (17-ps) phase is associated with a further spectral relaxation. Bleaching/SE around 683 nm is partially lost

and replaced by the 690-nm component, resulting in an asymmetric difference spectrum. In a first approximation, this spectrum can be described by a mixture of 683- and 690-nm states. It is in line with the triplet-singlet (T-S) spectrum, which also peaks at 685 nm at 77 K, but the T-S spectrum shows less intensity at the low-energy side and an additional minimum around 668 nm (Groot et al., 1995). The 17-ps time constant probably corresponds to the lifetime of 10 ps for a 684-nm state, deduced from the width of the zero-phonon hole at 4.2 K (Chang et al., 1994). Like their interpretation, we have assigned the observed 17-ps process to an energy transfer event. The slow rate must originate from a large distance and/or an unfavorable orientation for Förster energy transfer. The fact that part of the 683-nm component remains bleached cannot be explained by a thermal equilibrium (kT at 77 K corresponds to ~ 2.5 nm). A likely possibility would be that either the Chl 39–42 pair on the luminal or the Chl 35–48 pair on the stromal side, which both constitute the 683-nm component, is not in contact with the 690-nm state.

In contrast to the spectral changes on a faster timescale, the spectral changes associated to the 17-ps process are strongly nonconservative. The 690-nm state must carry an oscillator strength relative to the 683-nm state as low as ~ 0.6 to explain the overall loss of bleaching/SE (the final ratio of the population over the 683- and 690-nm pools equals then 1:3). The even more nonconservative change in the fluorescence spectrum associated with the 28-ps phase (Fig. 9) further supports the lower oscillator strength of the 690-nm state.

The low oscillator strength cannot have an excitonic origin. The observed slow time constant (17 ps) by which the 690-nm state is populated contradicts that this time reflects a relaxation from a state excitonically coupled to the 690-nm state. A very weakly coupled dimer (coupling much smaller than the disorder) was proposed (Chang et al., 1994), in which a 687-nm state relaxes ultrafast to the 690-nm state. We have found no evidence for such coupling. The protein and/or carotenoid environment could lower the oscillator strength of the 690-nm Chl, but this effect is not expected to be large enough to explain our observations. We therefore propose that the loss of oscillator strength is (partly) due to a transition from super-radiant states to the uncoupled 690-nm state, which has a normal oscillator strength. In our Monte Carlo simulations (note that the 690-nm dipole is outside the scope of our simulations due to its orientation), we indeed obtained larger oscillator strengths for the lower exciton states, which are populated at early times in our pump-probe experiments.

CONCLUDING REMARKS

In this work we have investigated EET in purified CP43 and CP47 complexes using time-resolved absorbance-difference and fluorescence spectroscopy. On a fast timescale, CP43

and CP47 behave very similarly, consistent with their structural homology. We observed an ultrafast relaxation of 0.2–0.4 ps, which we ascribed in both complexes to EET between Chls within the stromal layer. A fast rate of 2–3 ps is ascribed to EET from the luminal to the stromal side (CP43) and to EET to a specific luminal or stromal excitonic state (CP47). The state reached after a few picoseconds is almost identical in both complexes, displaying a narrow band at 682–683 nm. We conclude that excitation energy transfer within CP43 and CP47 is fast and therefore does not contribute significantly to the well-known slow trapping of excitation energy in photosystem II, thereby supporting the conclusion by Vasil'ev et al. (2001).

The Chl closest to a RC chlorin (number 26 for CP43 and number 43 for CP47, both ~ 21 Å from a pheophytin and a peripheral Chl) and the second closest (number 32 in CP43 and number 47 in CP47, both ~ 25 Å from a pheophytin) are located on the stromal side of the membrane. EET from the core antenna to the RC must therefore proceed from the stromal side of the membrane, as depicted in Fig. 12.

We thank Janne Ihalainen for help with the time-resolved fluorescence measurements with the streak camera, Markus Wendling for help with the Monte Carlo simulations, and Henny van Roon for the expert preparation of the CP43 and CP47 particles.

This research was supported by the Netherlands Organization for Scientific Research (NWO) via the Dutch Foundations for Earth and Life Sciences (ALW).

REFERENCES

- Barber, J., E. Morris, and C. Büchel. 2000. Revealing the structure of the photosystem II chlorophyll binding proteins, CP43 and CP47. *Biochim. Biophys. Acta.* 1459:239–247.
- Boekema, E. J., H. van Roon, F. Calkoen, R. Bassi, and J. P. Dekker. 1999a. Multiple types of association of photosystem II and its light-harvesting antenna in partially solubilized photosystem II membranes. *Biochemistry.* 38:2233–2239.
- Boekema, E. J., H. van Roon, J. F. L. van Breemen, and J. P. Dekker. 1999b. Supramolecular organization of photosystem II and its light-harvesting antenna in partially solubilized photosystem II membranes. *Eur. J. Biochem.* 266:444–452.
- Chang, H.-C., R. Jankowiak, C. F. Yocum, R. Picorel, M. Alfonso, M. Seibert, and G. J. Small. 1994. Exciton level structure and dynamics in the CP47 antenna complex of photosystem II. *J. Phys. Chem.* 98: 7717–7724.
- Dekker, J. P., E. J. Boekema, H. T. Witt, and M. Rögner. 1988. Refined purification and further characterization of oxygen-evolving and Tris-treated photosystem II particles from the thermophilic cyanobacterium *Synechococcus sp.* *Biochim. Biophys. Acta.* 936:307–318.
- Den Hartog, F. T. H., J. P. Dekker, R. van Grondelle, and S. Völker. 1998. Spectral distributions of “trap”-pigments in the RC-, CP47- and CP47 RC complexes of photosystem II at low temperature: a fluorescence line-narrowing and hole-burning study. *J. Phys. Chem. B.* 102: 11007–11016.
- Durrant, J. R., D. R. Klug, S. L. S. Kwa, R. van Grondelle, G. Porter, and J. P. Dekker. 1995. A multimer model for P680, the primary electron donor of photosystem II. *Proc. Natl. Acad. Sci. U.S.A.* 92:4798–4802.
- Fidder, H., J. Knoester, and D. A. Wiersma. 1991. Optical properties of disordered molecular aggregates: a numerical study. *J. Chem. Phys.* 95:7880–7890.

- Gobets, B., I. H. M. van Stokkum, M. Rögner, J. Kruijff, E. Schlodder, N. V. Karapetyan, J. P. Dekker, and R. van Grondelle. 2001. Time-resolved fluorescence emission measurements of photosystem I particles of various cyanobacteria: a unified compartmental model. *Biophys. J.* 81: 407–424.
- Gradinaru, C. C., S. Özdemir, D. Gülen, I. H. M. van Stokkum, R. van Grondelle, and H. van Amerongen. 1998. The flow of excitation energy in LHCII monomers: implications for the structural model of the major plant antenna. *Biophys. J.* 75:3064–3077.
- Gradinaru, C. C., I. H. M. van Stokkum, A. A. Pascal, R. van Grondelle, and H. van Amerongen. 2000. Identifying the pathways of energy transfer between carotenoids and chlorophylls in LHCII and CP29: a multicolor pump-probe study. *J. Phys. Chem. B.* 104:9330–9342.
- Groot, M.-L., R. N. Frese, F. L. de Weerd, K. Bromek, Å. Pettersson, E. J. G. Peterman, I. H. M. van Stokkum, R. van Grondelle, and J. P. Dekker. 1999. Spectroscopic properties of the CP43 core antenna protein of photosystem II. *Biophys. J.* 77:3328–3340.
- Groot, M.-L., E. J. G. Peterman, I. H. M. van Stokkum, J. P. Dekker, and R. van Grondelle. 1995. Triplet and fluorescing states of the CP47 antenna complex of photosystem II studied as a function of temperature. *Biophys. J.* 68:281–290.
- Jankowiak, R., V. Zazubovich, M. Rätsep, S. Matsuzaki, M. Alfonso, R. Picorel, M. Seibert, and G. J. Small. 2000. The CP43 core antenna complex of photosystem II possesses two quasi-degenerate and weakly coupled Q_y -trap states. *J. Phys. Chem. B.* 104:11805–11815.
- Kwa, S. L. S., S. Völker, N. T. Tilly, R. van Grondelle, and J. P. Dekker. 1994. Polarized site-selection spectroscopy of chlorophyll *a* in detergent. *Photochem. Photobiol.* 59:219–228.
- Monshouwer, R., M. Abrahamsson, F. van Mourik, and R. van Grondelle. 1997. Superradiance and exciton delocalization in bacterial photosynthetic light-harvesting systems. *J. Phys. Chem. B.* 101:7241–7248.
- Monshouwer, R., A. Baltuska, F. van Mourik, and R. van Grondelle. 1998. Time-resolved absorption difference spectroscopy of the LH-1 antenna of *Rhodospseudomonas viridis*. *J. Phys. Chem. A.* 102:4360–4371.
- Rhee, K.-H., E. P. Morris, J. Barber, and W. Kühlbrandt. 1998. Three-dimensional structure of the plant photosystem II reaction centre at 8 Å resolution. *Nature.* 396:283–286.
- Schatz, G. H., H. Brock, and A. R. Holzwarth. 1988. Kinetic and energetic model for the primary processes in photosystem II. *Biophys. J.* 54: 397–405.
- van Amerongen, H., and R. van Grondelle. 2001. Understanding the energy transfer function of LHCII, the major light-harvesting complex of green plants. *J. Phys. Chem. B.* 105:604–617.
- van Dorsen, R. J., J. Breton, J. J. Plijter, K. Satoh, H. J. van Gorkom, and J. Ames. 1987. Spectroscopic properties of the reaction center and of the 47 kDa chlorophyll protein of photosystem II. *Biochim. Biophys. Acta.* 893:267–274.
- van Grondelle, R., J. P. Dekker, T. Gillbro, and V. Sundström. 1994. Energy transfer and trapping in photosynthesis. *Biochim. Biophys. Acta.* 1187:1–65.
- van Leeuwen, P. J., M. C. Nieveen, E. J. van de Meent, J. P. Dekker, and H. J. van Gorkom. 1991. Rapid and simple isolation of pure photosystem II core and reaction center particles from spinach. *Photosynth. Res.* 28:149–153.
- van Stokkum, I. H. M., T. Scherer, A. M. Brouwer, and J. W. Verhoeven. 1994. Conformational dynamics of flexibility and semirigidly bridged electron donor-acceptor systems as revealed by spectrotemporal parameterization of fluorescence. *J. Phys. Chem.* 98:852–866.
- Vasil'ev, S., P. Orth, A. Zouni, T. G. Owens, and D. Bruce. 2001. Excited-state dynamics in photosystem II: Insights from the x-ray crystal structure. *Proc. Natl. Acad. Sci. U.S.A.* 98:8602–8607.
- Wilhelm, T., J. Piel, and E. Riedle. 1997. Sub-20-fs pulses tunable across the visible from a blue-pumped single-pass noncollinear parametric converter. *Opt. Lett.* 22:1494–1496.
- Zouni, A., H.-T. Witt, J. Kern, P. Fromme, N. Krauss, W. Saenger, and P. Orth. 2001. Crystal structure of photosystem II from *Synechococcus elongatus* at 3.8 Å resolution. *Nature.* 409:739–743.